International Journal of Computer Engineering and Data Science (ISSN: 2737-8543)
Volume 3–Issue 2, April –June 2023

Advances in temperature control for microelectronic measurements

Abdessamad Malaoui

Research Laboratory in Physics and Sciences for Engineer (LRPSI), Sultan Moulay Slimane University, Morocco

E-mail : a.malaoui@usms.ma

Article history

Received Aug 13, 2023
Revised Oct 02, 2023
Accepted Oct 06, 2023
Published Oct 18, 2023

ABSTRACT

This paper introduces an electronic temperature control system with the objective of delivering a functional prototype that is both cost-effective and capable of rapid and accurate performance. Intended for utilization in research laboratories for precise temperature control during electrical measurements, this device employs a 10-bit embedded system to implement the PID algorithm. The electronic schematics and results of this controller are discussed and compared to those of an earlier 8-bit controller and a standard laboratory regulator. Initial assessments focus on regulating the temperature of a photovoltaic junction to ascertain its intrinsic electrical characteristics. The results obtained vividly illustrate the extent and magnitude of the benefits conferred by this innovative device.

Keywords: ***Embedded system, Arduino, Peltier, Temperature control, PID command.***

I. INTRODUCTION

Temperature regulation is a crucial element in ensuring the reliability and accuracy of measurements within research laboratories. Fluctuations in temperature can significantly impact the stability and effectiveness of electronic devices, potentially leading to distortions in experimental results. Precise temperature control is vital for establishing consistent and reproducible experimental conditions, thereby enhancing scientific rigor and the credibility of research findings. Additionally, effective temperature management helps mitigate drift effects and prevents unexpected behaviors in electronic components [1]. The integration of advanced thermal management technologies, such as PID controllers, is essential for obtaining high-quality data. While previous research has predominantly focused on measurement aspects, this paper delves into the engineering dimension by proposing the use of embedded systems for temperature regulation. Specifically, we explore an electronic apparatus utilizing an Arduino microcontroller, Pelletier semiconductor wafers, and other components, aiming to achieve cost-effective, precise, and rapid temperature control [2]. Drawing inspiration from a previous 8-bit microcontroller-based system, we present a two-stage architecture involving power electronics and a programmable Arduino ATmega controller with PID algorithm [3]. This paper introduces a novel PID controller architecture, highlighting its benefits and comparing it with alternative temperature control methods. Moreover, the calibration process and a comparative analysis between the two electronic systems shed light on the influence of microcontroller resolution on temperature control performance. This study bridges the gap between measurement and engineering approaches, offering valuable insights into enhancing temperature regulation in electronic systems for improved experimental outcomes..

II. DESCRIPTION OF OLD TEMPERATURE REGULATORS

A. Conventional Temperature Control Apparatus.

Various laboratories possess conventional temperature control equipment. In our context, we employ a thermostat of the Ministat Huber type (DIN 12879-KI), which includes both heating and cooling pumps. This thermostat is capable of regulating temperatures within the range of -20°C to +100°C.

The described temperature control system operates on conventional principles, employing a heat-transfer fluid to regulate temperature. This mechanism involves the circulation of the fluid through metallic cylinders connected by insulated silicone pipes, creating a closed-loop thermal system. The specific thermostat model adopted, known as RCS6 by LAUDA, is characterized by a resistance thermometer (PT 500/PID) that aids in accurate temperature measurement and control. Notably, this thermostat incorporates a closed circuit designed to manage the fluid flow, allowing for efficient cooling and heating processes. The flow rates of 10/13 liters per minute and suction capacity of 8/9 liters per minute contribute to its effectiveness. This entire temperature control setup is computer-controlled, adding a layer of automation and precision. The system's operational range spans from -30°C to 150°C, enabling a wide scope of temperature control applications. It highlights the systematic approach to temperature regulation, encompassing

fluid dynamics, resistance thermometry, and computerized control, all contributing to the robust and versatile nature of the implemented system..

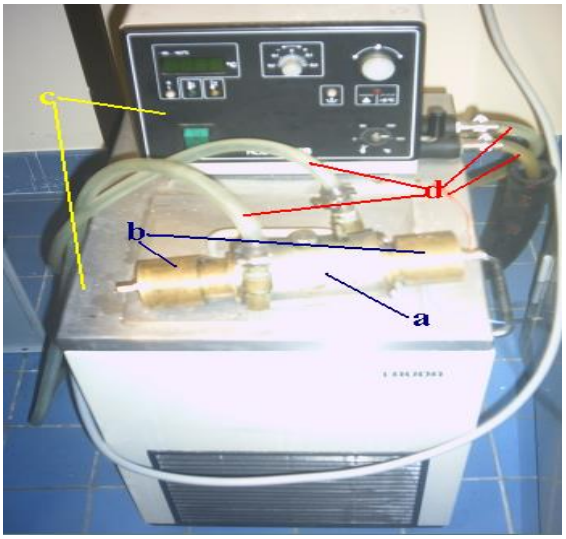

Figure 1. Old laboratory temperature regulator

(a) Two cylindrical cells, (b) Connector/support for the test junction, (c) Ministat temperature servo, and (d) Circulating liquid pipes.

B. *Electronic Controller Utilizing an 8-Bit Microcontroller*

Our research team's initial endeavor in this domain to enhance temperature control dates back to 2004. This project was executed utilizing an 8-bit programmed chip. The diagram below depicts an architecture centered around the ST microcontroller family, featuring two distinct processes: one employing the Joule effect for heating and the other utilizing the Pelletier effect for cooling. Due to limitations in the programmable component's capabilities, we had to partition the PID controller into two segments: the first in the external hardware of the microcontroller (µC), and the second within the program section. Subsequent enhancements were made to the aforementioned system, as explored in various studies [4]. Several architectures were tested and implemented to optimize the temperature control performance.

The ST62xx microcontroller, developed by SGS-Thomson Company, emerges as a pivotal element in the programmable hardware controller. Its inclusion, boasting 64 bytes of data memory RAM, empowers efficient data handling and manipulation. The accompanying EPROM, with a notable capacity of 3872 bytes, provides ample space for storing essential program instructions and data. The microcontroller's versatility is further evident with its integration of 20 analog-to-digital converter pins, enabling seamless conversion of analog signals to digital data for processing. This comprehensive array of features encapsulates the microcontroller's significance in enabling sophisticated temperature regulation and precise control within electronic systems, underscoring its role in enhancing performance and reliability.

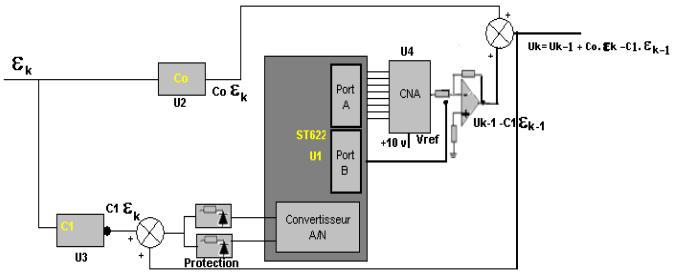

Figure 2. 8-bits temperature regulator

III. MEASUREMENT ASSEMBLY

A. *Realized electronic device*

The central component of the electronic implementation is the ST62xx microcontroller, developed by SGS-Thomson Company. This microcontroller encompasses RAM and EPROM memory, a Timer, three ports (A, B, and C) configured for input/output, and 20 Analog-to-Digital (A/D) converters. The temperature sensor employed is the AD590, which generates an output current proportionate to absolute temperature. With a sensitivity of one µA /°K, it operates within a temperature range of -55°C to 150°C. The A/D conversion of electrical signals is carried out through port C. Specifically, pin PC4 serves as the input for the set point through stage U5, while pin PC7 receives the positive error loop of regulation via U8, and pin PC5 receives the negative error via U9.

For precise current-to-voltage conversion, the operational amplifier OP27 was chosen due to its exceptional stability and reliability. Its output correlates with absolute temperature. The desired temperature set point is generated by a precision potentiometer. Diodes (D1, D2, and D3) and 330-ohm resistors are employed to adapt and protect the inputs of the ST6225. Ports A and B are respectively utilized to control the heating and cooling electronics.

B. *Designed thermal system*

The thermal system constructed takes on the shape of a parallelepiped, measuring 175x50x50 mm³, made from brass material [2]. It consists of a cylindrical chamber that holds a liquid to be tested using ultrasonic waves. On its lateral faces, thermoelectric plates are affixed. The ultrasonic transducers, responsible for generating and receiving acoustic waves, are crafted from ceramics (titanate-zirconate) with a resonance frequency of 5 MHz [5].

A schematic diagram of the cell and its two thermal components is presented. Φ represents the heat flow dissipating through the cell's surface area (S) to the surroundings.

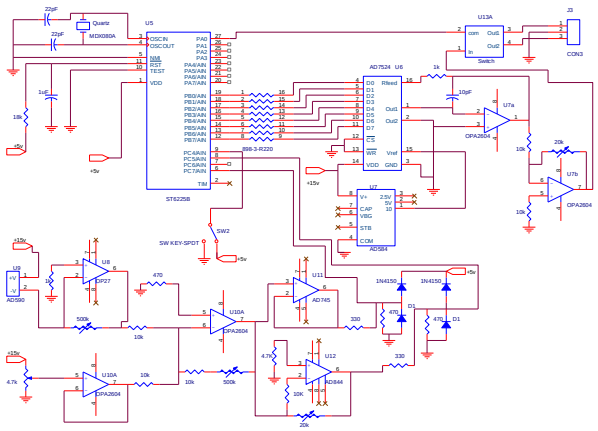

Figure 3. Electronic schematic diagram of the realized control assembly

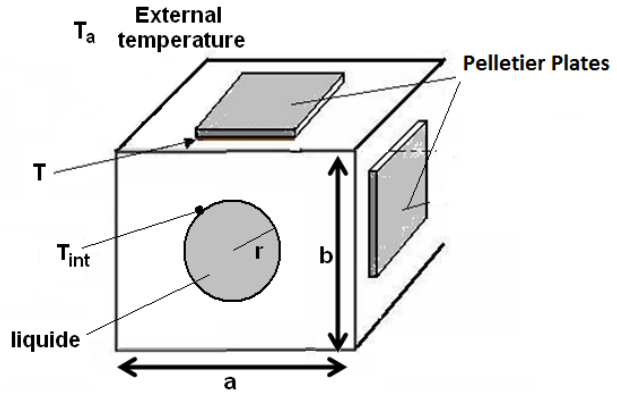

Figure 4. Synoptic schematic of thermal cell

Considering heat losses to the surrounding ambient with a temperature denoted as Ta, the resultant power can be expressed as [6]:

$$P - \Phi = P - h.S(T - T_a) = C.\frac{dT}{dt} \quad (1)$$

Here, (h) represents the heat exchange coefficient between the metal and the surrounding air (W/m².°C), while C stands for the total heat capacity, and (P) signifies the electric power supplied to the system in Watts. The initial and final temperatures can be determined as indicated by [6]:

$$T_1 = T_a + \frac{P}{h.S} \quad (2)$$

and

$$\phi_L = 2.\pi.\frac{L.\lambda_L.(T_{int} - T)}{\ln[\frac{b}{r}(0.637 - 1.781e^{-2.9\frac{a}{b}})]} \quad (3)$$

The Φ_L represents the power transfer occurring between the inner and outer surfaces of the ultrasonic cell, with temperatures Tint and T respectively. Meanwhile, L corresponds to the length of the cell.

In light of these equations, the system displays nonlinearity and incorporates variable components contingent on experimental conditions and the liquid medium employed. The precise model for power losses with the external medium remains elusive. Consequently, devising a static model programmable via the ST microcontroller proves challenging. To address this issue, we employ an experimental approach for modeling.

C. Processes modelling

The Strejc and Broïda techniques are employed to derive the transfer functions for individual processes [7]. A signal with an amplitude of ±10% of the nominal value is applied to the input of each subsystem. This yields a first-order function as the outcome:

$$H(p) = K_o.\frac{e^{-p.T_r}}{1 + \tau.p} \quad (4)$$

Where Ko, Tr, and τ represent the static gain, delay, and time constant, respectively. The parameters of the transfer function for the heating and cooling processes are influenced by the liquid medium within the cylindrical cavity. Two mediums, namely air and water, are utilized to establish the system model. The selection of a controller should align with the desired specifications, typically influenced by the value of θ = τ/ Tr [7].

IV. PROPOSED ELECTRONIC REGULATOR WITH ARDUINO

In the proposed electronic system, a 10-bit microcontroller is employed to address the limitations of the 8-bit µC. The embedded system utilized in this study is an Arduino Atmega, developed by Atmel Company, offering a range of advantages including memory size, word processing capabilities, speed, port count, addressing modes, and other specifications. These advantages permit a departure from the regulatory architecture dictated by the previous µC. Each step of the PID algorithm is implemented as a program, as illustrated in the block diagram. Numerous parameter tests were conducted on this controller. In our scenario, the Proportional (P) and Integral (I) actions suffice to yield satisfactory outcomes. The transfer function C(s) of a PI analog controller is expressed as:

$$C(s) = K_p + \frac{K_i}{s} \quad (5)$$

Where s is the Laplace variable and K_p and K_i are the proportional and integral gains, they are given by Ziegler-Nichols method. The discrete form for PI controller is:

$$C(z) = K_p \quad \frac{K_i.T_e}{2} + \frac{K_i.T_e}{1 - Z^{-1}} \quad (6)$$

T_e is the sampling period, used in the bilinear transformation :

$$s = \frac{2}{T_e}.\frac{z-1}{z+1} \quad (7)$$

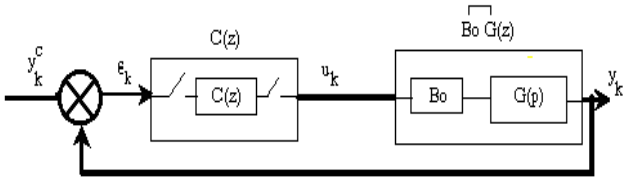

Figure 5. Block diagram of the controller used by Arduino

The embedded system is programmed to oversee both the Pelletier plates for heating and cooling through a unified mechanism. This approach distinguishes itself from the methodology employed by the ST62 µC, as mentioned in Section II. Control over both thermal processes is achieved via a set of electronic components (operational amplifiers, TEC transistors, D/A and A/D converters, etc.). The temperature sensor in use (AD590) exhibits a sensitivity of 1 µA /°K within the temperature range of -55°C to 150°C. The power electronics for cooling and heating leverage the Thermoelectric Cooler or "TEC" component, employing the Pelletier effect discovered in 1834, which reverses the direction of electrical current. This effect relies on a thermoelectric material, specifically a semiconductor junction known as "bismuth telluride." The Pelletier plates demand substantial input power, typically around 80 Watts, translating to approximately 6 amps at 16 VDC, for instance.

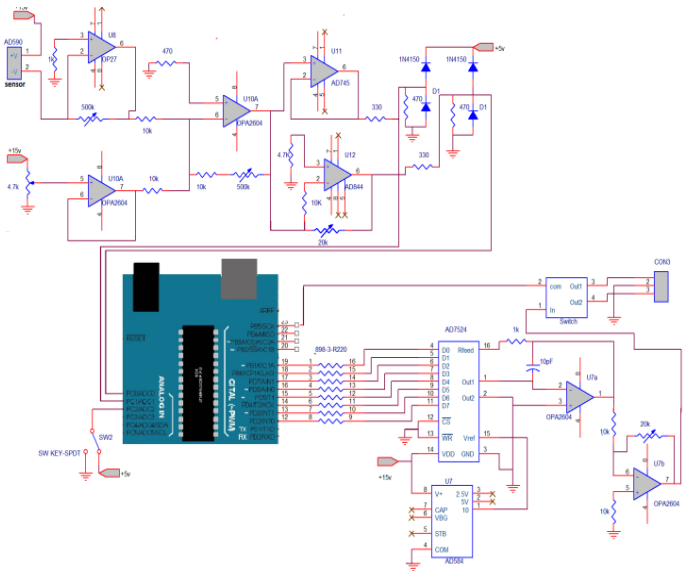

Figure 6. Electronic schematic diagram of the control assembly

For this purpose, an adjustable switching power supply can be employed. In our system, we utilize the CP0.8-31-06 model, which encompasses the subsequent attributes:

TABLE I. CARACTERISTIQUES ELECTRIQUE DES PLAQUES DE PELTIER

Max Current (A)	*Power (W)*	*Max Voltage (V)*
2.1	4.4	3.75

Each side of the Device Under Test (DUT) carrier is equipped with four Pelletier plates for heating and six Pelletier plates for cooling, connected in series. The combined power of the four plates is approximately 16 Watts, resulting in a total power output of around 100 Watts.

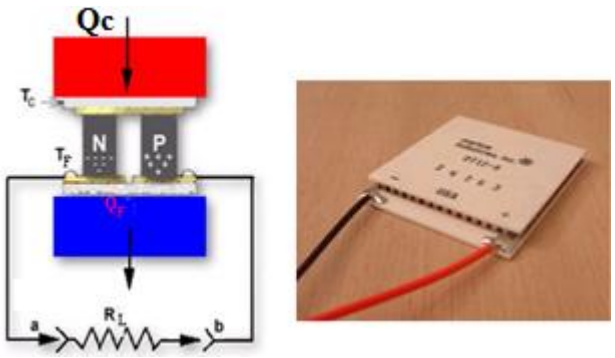

Figure 7. Electronic diagram and image of the used Peltier plate

The voltage in its pins is:

$$U = n.[\alpha.(T_C - T) + R_p.I_p] \quad (8)$$

$$R_p = \rho.\frac{e_s}{S_e} \quad (9)$$

Where n, α, ρ, e_s and S_e are constants of the Pelletier plates, T_c it's a hot face temperature. The Thermoelectric junctions of Pelletier are managed by the following laws:

- The cooling capacity (PF) absorbed by the cold face of the Pelletier is expressed as:

$$P_F = n.[\alpha.I.T_F - \frac{1}{2}.R.I^2 - K.(T_C - T_F)] \quad (10)$$

- The heat capacity (PC) generated by the hot face is:

$$P_C = n.[\alpha.I.T_C + \frac{1}{2}.R.I^2 - K.(T_C - T_F)] \quad (11)$$

- The electric power (PE) provided to the cell is:

$$P_E = P_C - P_F = n.[\alpha.I.(T_C - T_F) + R.I^2] \quad (12)$$

- The voltage (U) to the cell terminals:

$$U = n.[\alpha.(T_C - T_F) + R.I] \quad (13)$$

n : Number of the cell blocks.

α : Seebeck coefficient by paved in volts /°K.

I : Current through the cell.

k : Thermal conductivity in watts/°K.

T_F : Temperature of the cold face in °K.

T_C : Temperature of the hot face in °K.

The output voltage of the generators without load is:

$$V = S.\Delta T \tag{14}$$

(S =n.α) is the average Seebeck coefficient in volts/°K. If a load is connected to the thermoelectric, the output voltage decreases. The output current is:

$$I = \frac{S.\Delta T}{R_C + R_L} \tag{15}$$

R_c : Mean internal resistance of thermocouples (Ohms).

R_L : Load resistance (Ohms).

This assembly represents a power electronic system utilizing Pelletier plates, which relies on a thermoelectric material known as TEC—a semiconductor junction employing "Tellurium of Bismuth." The regulation of current through the Pelletier thermoelectric plates is governed by the voltage at the J1 jumper. The manipulation of this voltage is achievable through the adjustment of P1, which dictates the amplification factor of the U2A amplifier.

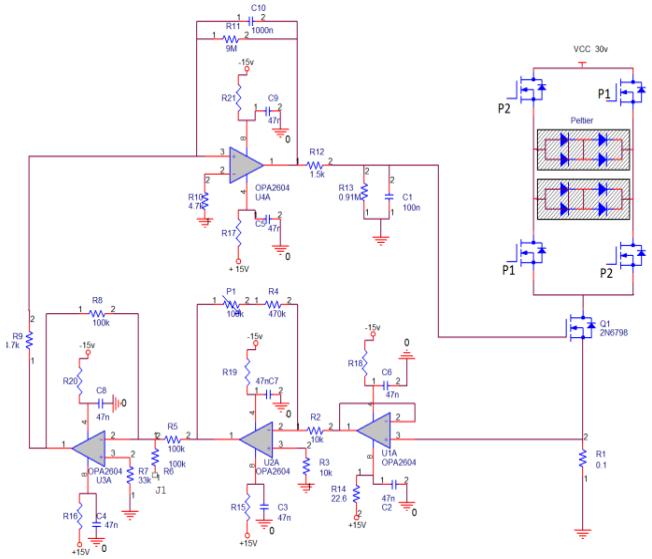

Figure 8. Schematic of heating and cooling power electronics.

L'élément électronique initial, U1A, assume le rôle d'adaptateur d'impédance en surveillant la chute de tension aux bornes de la résistance R1. Cette tension reflète fidèlement le courant circulant dans les charges. Suite à cela, le deuxième composant, U2A, fonctionne comme un amplificateur de tension pour ce signal, avec son facteur d'amplification déterminé par les résistances R2, R3, R4 et P1. Un amplificateur supplémentaire, U3A, fonctionne comme un additionneur, limitant efficacement la tension de sortie de U2A à l'aide d'une tension de commande en J1.

U4A sert d'intégrateur, où C20 et R39 se voient attribuer des valeurs significatives pour obtenir simultanément un gain statique élevé et une constante de temps prolongée pour le processus d'intégration. De plus, le filtre R13//C1 est intégré pour supprimer les oscillations à haute fréquence.

La régulation du courant thermoélectrique est orchestrée par une commande de tension appliquée à la grille d'un transistor FET, fonctionnant dans une configuration en boucle fermée établie par un amplificateur opérationnel (Op Amp). La modification de la polarisation électrique des modules Peltier est facilitée par quatre FET configurés en pont en H. Ces FET, contrôlés par les broches P1, P2, P3 et P4, orchestrent l'inversion de polarisation, permettant ainsi la transition transparente entre les modes de refroidissement et de chauffage des plaques Peltier. L'ensemble de ce processus est géré par un système de contrôle unifié..

V. RESULT AND DISCUSSIONS

Processes modelling are made by “Strejc” and “Broïda” methods. These are used to find the transfer functions of two processes. The input of thermal system is a step signal with ±10%. The results are the functions of first order:

$$H(s) = K_o.\frac{e^{\ T_r.s}}{1+\tau.s} \tag{16}$$

Where K_o , T_r and τ are static gain, delay and time-constant respectively.

To solve the problem of the non-symmetry in our system, two application forms of PI controller are proposed.

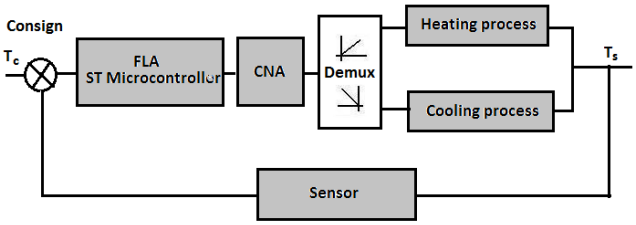

Figure 9. Schematic of heating and cooling controller.

The values of the PI controller parameters are determined by an experimental attempt and the two algorithms are tested and their specifications are compared. We tested several gain values (Kp and Ki), the results obtained are presented in the following table.

TABLE II. VARIOUS VALUES OF PI CONTROLLERS.

Process	Kp	Ki	Max overshoot	Stability time ts (second)
Cooling	2,686	0,0107	300%	300
Heating	0,176	0.0009	25%	450

The comparison reveals the enhancements achieved by the Arduino-based electronic system on multiple fronts. Notably, a 10-fold improvement in static error and a nearly 20-fold increase in speed are observed when compared to the "Ministat" system.

TABLE III. PARAMETERS OF THE AIR TRANSFER FUNCTIONS.

Type of regulator	Process	Time constant (seconds)	Static error
Laboratory controller	Heating	2081	10%
	Cooling	2509	
8-bit controller	Heating	161.2	5%
	Cooling	210.8	
Arduino controller	Heating	102	1%
	Cooling	115.4	

Furthermore, it operates at approximately 1.5 times the speed of the 8-bit controller. The updated measurement system offers additional advantages compared to the previous system (Ministat). The table below outlines the key enhancements.

TABLE IV. ADVANTAGE OF PROPOSED CONTROL / MINISTAT

Specification	Improvement (times)
Cost	5
Speed	10
Noise	300
Volume	50
Consumption	8
Weight	34
Stabilty	10

To assess the reliability of the implemented system, we conducted measurements of the ultrasonic speed (Vm) and subsequently compared the obtained results with the established reference of Del Grosso (Vref) [8].

TABLE V. MEASURED AND ERRORS ULTRASONIC SPEEDS VALUES.

T °C	1	10	25	60	95,1
Vm (m/s)	1407,30	1447,24	1496,61	1550,98	1547,09
Error (m/s)	0,06	0,03	0,03	0,02	0,02

We conducted a comparative analysis of these findings by employing the standard deviation (SD) and assessing the maximum velocity error. The ensuing table provides an encapsulation of the juxtaposition between our acquired results and those derived from Del Grosso's data across different temperature ranges: low, medium, and high. Notably, there was a decrease in the standard deviation as the temperature increased. The maximum variation (ΔVmax) measured at 0.06 (m/s). Particularly noteworthy is the fact that the SD remains below 0.055 within the temperature range of 19°C to 95.1°C, thereby substantiating the precision of our conducted measurements.

TABLE VI. ERRORS OF ACOUSTIC SPEED BETWEEN MEASUREMENT AND REFERENCE [8].

T °C	0,5 < T < 10	19 < T < 45	60< T <95,1
Vm (m/s)	0,298	0,055	0,039
Error (m/s)	0,596	0,323	0,005

VI. CONCLUSION

This paper has explored the development and deployment of a cost-effective, programmable electronic instrument tailored for achieving precise and rapid temperature control, leveraging the PID algorithm. This innovative solution taps into the capabilities of a readily available 10-bit embedded system in the market, specifically the Arduino DAC. Moreover, we conducted a comprehensive comparative analysis by juxtaposing it with an alternative electronic configuration centered around an 8-bit microcontroller from the ST Microelectronics family. Our findings unequivocally underscore the substantial impact of the bit count in an electronic processing system on the overall performance and efficiency of the temperature control system. In parallel, the system devised in this study exhibits extensive potential applications across diverse industries and sectors, namely:

- Industrial Automation: This system proves invaluable for maintaining precise temperature control in industrial environments, where specific temperature ranges are paramount for processes such as manufacturing, chemical reactions, and food production.
- Laboratories and Research: Laboratories conducting experiments requiring meticulous temperature control, encompassing fields like biology, chemistry, and materials science, stand to benefit immensely. Future research avenues may delve into tailoring the system to accommodate specific laboratory equipment and integrating it with data logging and analysis tools.
- Greenhouses and Agriculture: Implementation of this technology in greenhouse environments augments plant growth through meticulous temperature and humidity control. Potential enhancements could involve integrating weather forecasts for even finer control.
- Residential Applications: Upgrading home air conditioning systems with this technology holds promise for energy savings and enhanced comfort. Further development could consider factors such as occupancy detection and integration with smart home ecosystems.
- Medical and Healthcare: The system's precision temperature control finds critical applications in medical equipment, pharmaceutical storage, and patient care. Customization for healthcare applications may necessitate compliance with stringent regulatory standards and the incorporation of fail-safe mechanisms.
- Energy Efficiency: To address sustainability concerns, optimizing the system for energy efficiency is imperative. Incorporating machine-learning algorithms to predict temperature changes and adjust accordingly can significantly reduce energy consumption.
- Education and Training: The developed system can serve as a valuable educational tool for students and professionals in electronics and automation fields. Designing user-friendly interfaces and educational resources can facilitate widespread adoption.

The cost-effective and programmable temperature control system presented in this article unlocks a multitude of opportunities across various sectors. By remaining responsive to user feedback and staying attuned to technological advancements, the system can evolve to meet the ever-growing demand for precise temperature control in our increasingly interconnected world.

REFERENCES

[1] Abdessamad Malaoui. "Precise electric measurèments with temperature using 10-bit embedded system: Application on photovoltaic junctions". International Conference on Microelectronics (ICM'15), pp.265-268, (2015)

[2] Malaoui Abdessamad, Quotb Kamal, Ankrim Mohamed, Benhayoun Mohamed. " Accurate temperature control of a ultrasonic cell using a microcontrolor". IEEE International Symposium on Industrial Electronics, ISIE04, 2004, pp. 231-235.

[3] A. Malaoui, "Automatisation en température par microcontrôleur d'un banc de mesure ultrasonore: Applications au contrôle qualité en agroalimentaire.", thèse de doctorat de l'Université de Provence, 2005.

[4] VODA A. A.. Landu I.D. A. "Method of the Auto-calibration of PID Controllers". Automatica. 1995, Vol.31. N 1.pp. 41-53.

[5] Wang, Haifeng & Jiang, Wenhua & Cao, Wenwu. (1999). Characterization of lead zirconate titanate piezoceramic using high frequency ultrasonic spectroscopy. Journal of Applied Physics. 85. 8083 - 8091. 10.1063/1.370646.

[6] Abdessamad Malaoui, "Measurement and modeling of electronic signature of Argan oil by non-destructive acoustic technique," International Journal of Innovation and Applied Studies, vol. 16, no. 4, pp. 902–913, June 2016.

[7] Byrski, Witold. (2017). A new method of multi-inertial systems identification by the Strejc model. 536-549. 10.1007/978-3-319-60699-6_52.

[8] V. A. Del Grosso, C. W. Mader. "Speed of sound in pure water", Acoust. Soc. Am Journal, Vol. 52, N° 5 (Part2), pp. 1442-1446, 1972.